Supporting Information

Highly efficient photoelectrocatalytic oxidation of arsenic(III) with polyoxometalate-thiacalix[4]arene-based metal-organic complex modified bismuth vanadate photoanode

Yuting Song,[a] Jia-Yi Zhang,[a] Jin Yang,*[a] Tao Bo *[b] and Jian-Fang Ma *[a]

[a] *Key Laboratory of Polyoxometalate and Reticular Material Chemistry of Ministry of Education, Department of Chemistry, Northeast Normal University, Changchun 130024, China*

[b] *Engineering Laboratory of Advanced Energy Materials, Ningbo Institute of Materials Technology and Engineering, Chinese Academy of Sciences, Ningbo 315201, China*

*Corresponding author

E-mail: yangj808@nenu.edu.cn (J. Yang)

Email: botao@nimte.ac.cn (T. Bo)

E-mail: majf247@nenu.edu.cn (J.-F. Ma)

Characterizations and instruments

All chemicals were commercially available. Thermogravimetric analysis is performed on a PerkinElmer TG-7 analyzer under N_2. Fourier transform infrared (FTIR) spectra were recorded on a Nicolet 6700 instrument. Powder X-ray diffraction (PXRD) patterns were measured on a Rigaku Dmax 2000 X-ray diffractometer with graphite monochromatized Cu Kα radiation (λ = 1.541 Å). Elemental analysis data was achieved on a Euro Vector EA3000 elemental analyzer. Valence band X-ray photoelectron spectroscopy (VB-XPS) was determined on a FEI ESCALAB Xi+ with an Al Kα radiation. Ultraviolet-visible diffuse reflectance spectra (UV-vis DRS) were recorded on a UV-visible-near-IR spectrophotometer (Varian Cary 500). Field emission scanning electron microscope (Hitachi SU-8010) was used to give the morphology of the samples. Transmission electron microscopy (TEM) images were achieved with a JEM-2100F transmission electron microscope (JEOL, Japan) at 200 kV (Since it is not feasible to test TEM of **1@BVO** on the FTO electrode, the sample of **B1-20** was removed from the FTO and prepared by ultrasonic dispersion with ethanol). Photoluminescence (PL) spectra were analyzed with fluorescence spectrometry (Hitachi F-4600). Electron spin resonance (ESR) experiments were implemented on a Bruker EMX-PLUS. As(V) concentrations were detected with UV-visible absorption spectroscopies (Varian Cary 50 UV-visible spectrometer).

X-ray crystallography

An Oxford diffraction Gemini R CCD diffractometer with graphite-monochromated Mo Kα radiation (λ = 0.71073 Å) was used to collect the single-

crystal XRD data. The crystal structure was solved and refined by full matrices methods against F^2 using SHELXL-2018/3 program package and Olex2-1.5 software.[1-3] The highly disordered solvents were removed by applying the SQUEEZE routine in PLATON.[4] CCDC deposition number is 2294354.

Experimental methods

Synthesis of $[Ag_2L(HL)][PW_{12}O_{40}]\cdot 2C_2H_5OH\cdot 2CH_3CN$ (1)

The thiacalix[4]arene ligand with four 5-mercapto-1-methyltetrazole groups (L) was prepared according to the literature.[5] A mixture of L (12 mg, 0.01 mmol), $H_3PW_{12}O_{40}\cdot xH_2O$ (29 mg, 0.01 mmol), $AgNO_3$ (7 mg, 0.04 mmol) and HNO_3 (2.3 M, 200 μL) was added to a solution of C_2H_5OH/CH_3CN (8 mL, 6/2, v/v) in a Teflon reactor (15 mL). The resulting mixture was heated at 120 °C for 3 days. After cooling to room temperature, colorless block crystals of **1** were achieved in a 53% yield based on L. Element analysis (%) calculated for $C_{120}H_{163}Ag_2N_{34}O_{50}PS_{16}W_{12}$: C 24.65, H 2.81, N 8.14; found: C 24.36, H 2.72, N 8.39. IR data (KBr, cm^{-1}): 3420(w), 2959(w), 1619(w), 1434(w), 1383(w), 1265(w), 1177(w), 1080(m), 977(m), 895(m), 817(s), 699(w), 507(w).

Fabrication of 1@BVO photoanodes

An electrodeposition-annealing method was applied to fabricate **BVO** on FTO substrate with active area of 1.8 × 2 cm^2.[6] Typically, $Bi(NO_3)_3\cdot 5H_2O$ (2 mmol) was added to KI solution (50 mL, 0.4 M, pH 1.6), and then mixed with *p*-benzoquinone ethylalcohol (20 mL, 0.23 M) to yield electrolyte. Using the above electrolyte, BiOI was prepared by electrodeposition in the potential range from -0.13 to 0 V *vs*.

Ag/AgCl. Subsequently, dimethyl sulfoxide (DMSO) solution with 0.5 M vanadyl acetylacetonate was added in drops to the BiOI and treated at 450 °C for 2 h. The **BVO** photoanode was gained after the resulting sample was soaked in 1 M NaOH for 40 min and washed with the distilled water.

1@BVO photoanode was prepared by a simple physical drop-casting method. Specifically, the sample of **1** (5 mg) was immersed in a mixture of 20 μL Nafion (5 wt %) and 180 μL ethanol, and then treated with ultrasound for 30 min at room temperature. The **1@BVO** photoanode was prepared by dropping the suspension onto the **BVO** photoanode. The resulting **1@BVO** photoanodes were named as **B1-X**, where X represents the dosage (μL) of the suspensions.

Photoelectrochemical measurements

Photoelectrochemical test was conducted on an electrochemical workstation (CHI 760E) and a 300 W Xenon lamp (PLS-SXE300) equipped with AM 1.5G filter (100 mW/cm^2). **1@BVO** photoanode was used as working electrode. The saturated calomel electrode (SCE) and Pt wire were respectively used as reference electrode and counter electrode. The supporting electrolyte was 0.5 M aqueous solution of Na_2SO_4. Under the simulated sunlight, time-dependent dynamic photocurrent response was analyzed at 0.3 V (vs. SCE). Electrochemical impedance spectroscopy (EIS) was measured at 0 V with the frequencies from 10^6 to 0.1 Hz. The linear sweep voltammetry curve was determined in the range from 0 to 1 V (vs. SCE).

Photoelectrocatalytic oxidation from As(III) to As(V)

The experiment for photoelectrocatalytic oxidation of As(III) was determined in

a quartz reactor with 50 mL Na_2SO_4 solution (0.1 M) containing 25 mg/L $NaAsO_2$ under the simulated sunlight at room temperature. The as-prepared **1@BVO** was employed as photoanode. Pt wire and SCE were respectively used as photocathode and reference electrode. Before photoelectrocatalytic experiments, the mixture was stirred in darkness for 60 min to ensure the adsorption-desorption equilibrium of As(III). Every 10 min after the irradiation, *ca.* 1 mL solution was taken out, and the concentrations of As(V) were recorded by colorimetric molybdene blue method.[7] Photoelectrocatalytic As(III) removal efficiency (%) was calculated on the basis of $A_t/A_{total} \times 100\%$, where A_t represents the corresponding absorbance of As(V) at the reaction time t, and A_{total} is the total arsenic absorbance in the solution. A_{total} is obtained when As(III) is completely oxidized to As(V) by adding $KMnO_4$ solution.

Estimation of the faradaic efficiency

The faradic efficiency of As(III) oxidation with **B1-20** photoanode was calculated with mnF/jt × 100%, where m represents the number of As(V) moles at the reaction time t, F is the faradic constant, n represents the number of the requirement electrons for the As(III) oxidation reaction ($n = 2$), and j is the average current density during the reaction.[8] Photocurrent of **B1-20** was gained in a mixed solution of Na_2SO_4 (0.1 M) and As(III) (25 mg/L) at 0.6 V (vs. SCE) under the simulated sunlight. Corresponding As(V) mole number was recorded by colorimetric molybdene blue method with UV-visible absorption spectroscopy.

Calculation details

Density functional theory (DFT) calculations were performed as implemented in

the Vienna Ab-Initio Simulation Package (VASP).[9] The interaction between the nucleus and the electrons was described by the projector augmented wave (PAW) method,[10] and the Perdew-burke-Ernzerh of the generalized gradient approximation (PBE-GGA)[11] exchange-correlation functional was employed. The plane-wave cutoff energy was set to be 550 eV and the Gaussian electron smearing method with σ = 0.10 eV was used. Due to the large size of the simulation system (including 368 atoms), the Monkhorst-Pack *k*-point mesh[12] (4 × 3 × 3) is large enough to achieve the required accuracy. The convergence criterion for the self-consistent field iteration of the system is 1×10^{-6} eV, and the atomic positions were fully relaxed until the maximum force on each atom is less than 0.02 $eVÅ^{-1}$. The DFT-D3 dispersion correction method[13] was used to treat the long-range dispersion interactions.

Supporting Figures

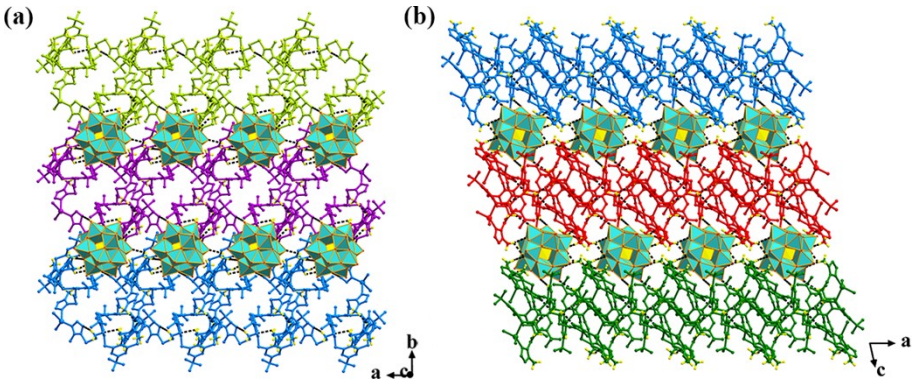

Fig. S1 2D supramolecular layer in (a) *ab* and (b) *ac* plane formed by hydrogen bonds.

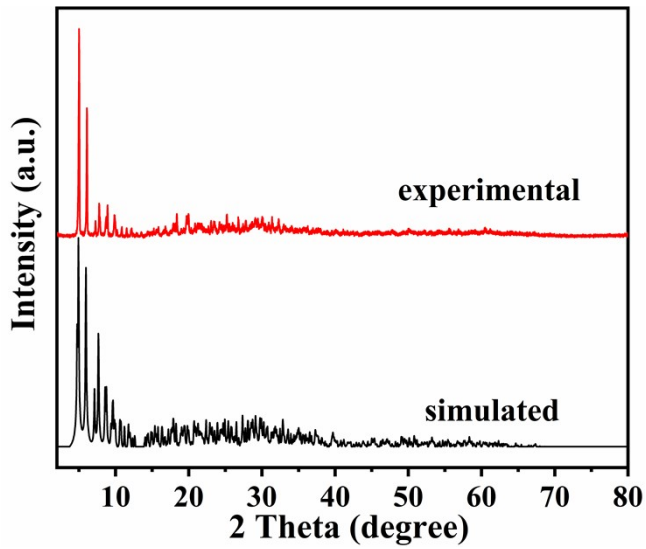

Fig. S2 PXRD patterns of **1**

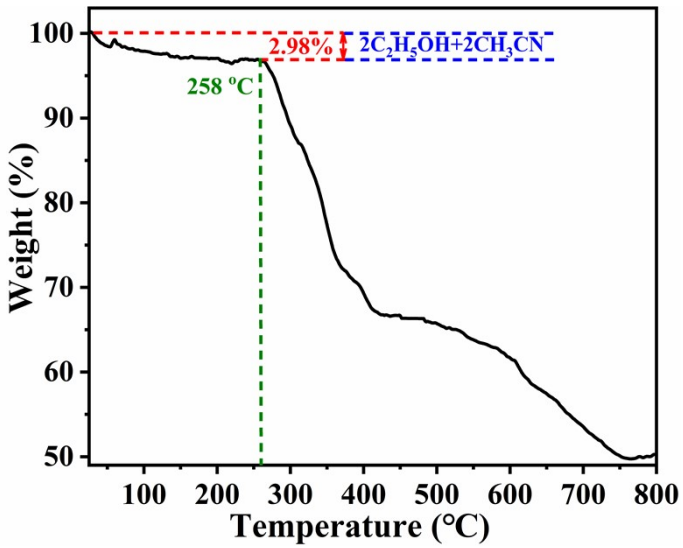

Fig. S3 TGA curve of **1**

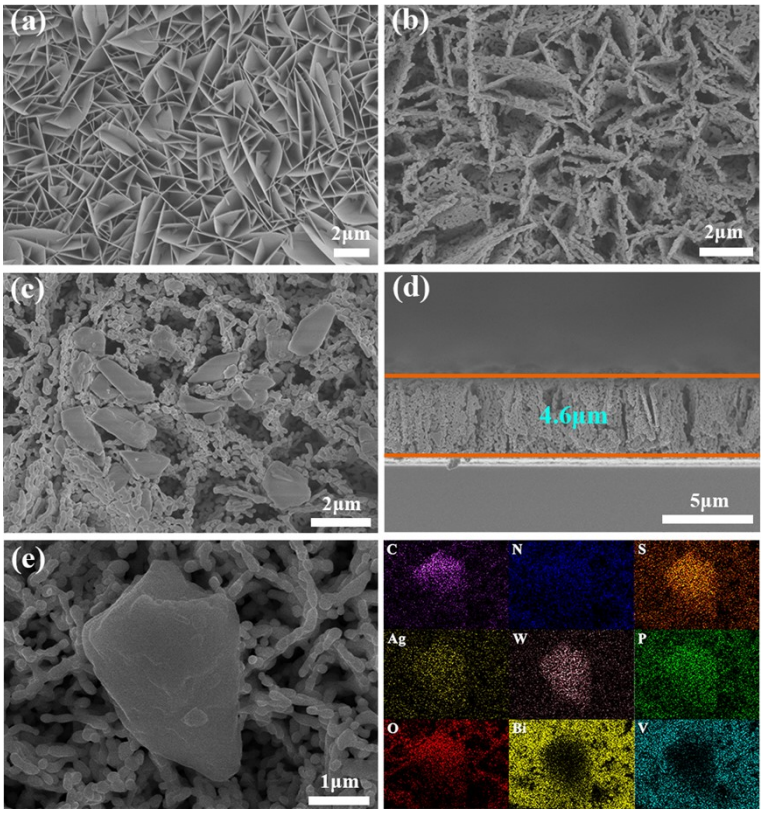

Fig. S4 SEM images of (a) **BiOI**, (b) **BVO** and (c) **B1-20**, (d) cross-sectional image of **B1-20** and (e) elemental mappings of **B1-20**.

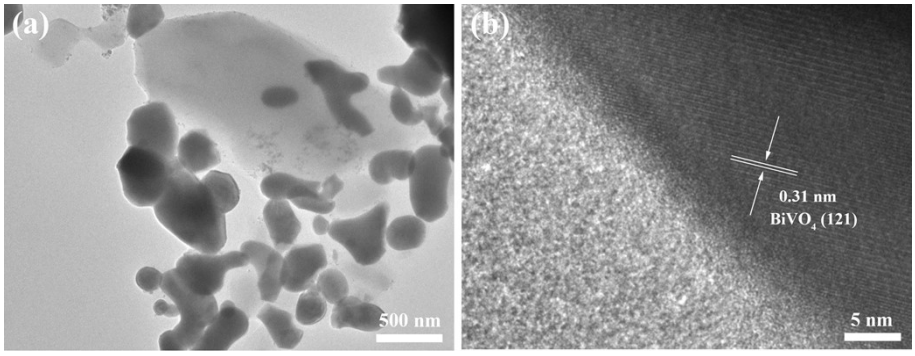

Fig. S5 (a) TEM image of **B1-20**, and (b) HRTEM image of **B1-20**.

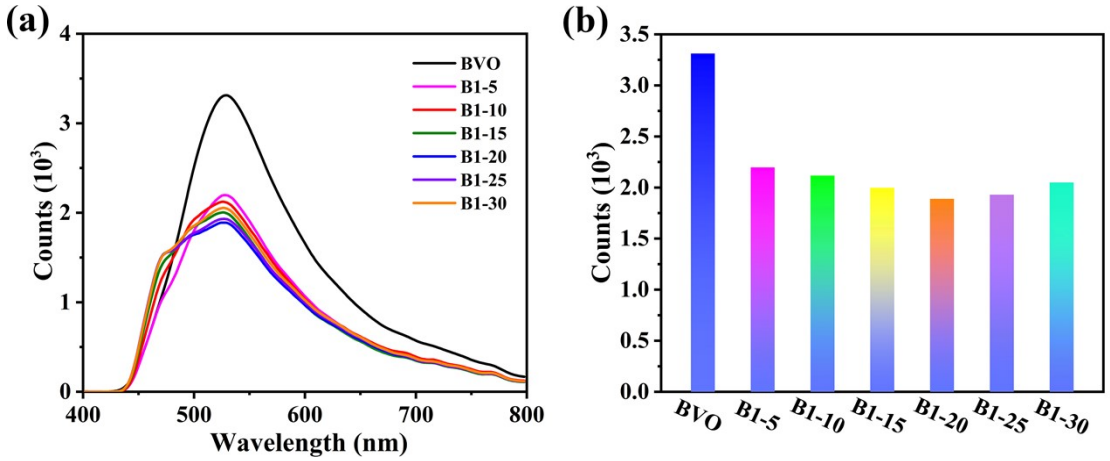

Fig. S6 (a) Steady-state photoluminescence spectra of **BVO** and **B1-X**, (b) the emission photoluminescence intensity of **BVO** and **B1-X** at 530 nm.

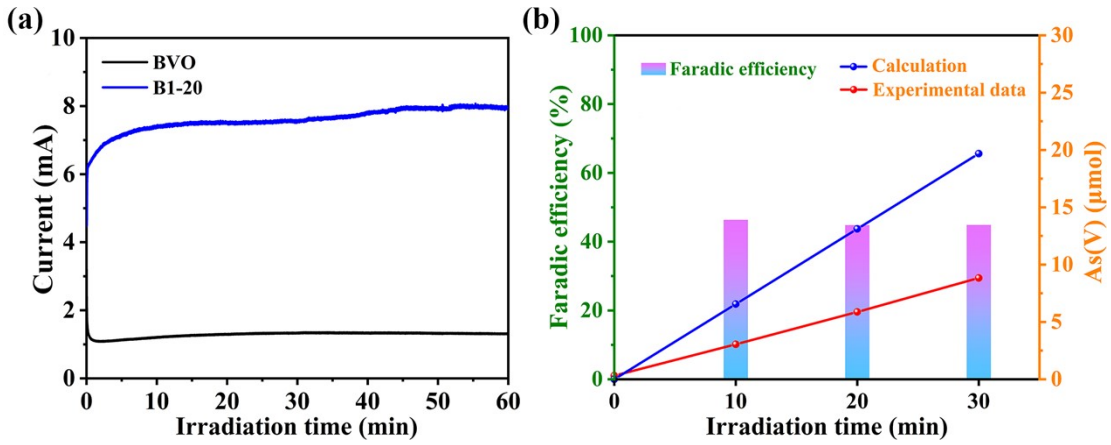

Fig. S7 (a) Photocurrents of **B1-20** and **BVO** in 0.1 M Na_2SO_4 solution containing 25 mg/L As(III) in the PEC process, (b) theoretically calculated and experimentally measured photoelectrocatalytic generation of As(V) on **B1-20**.

Fabrication of BL-20 photoanode

The ligand L (2.2 mg) was immersed into a mixture of 20 μL Nafion (5 wt %) and 180 μL ethanol. The mixture was treated with ultrasound for 30 min at room temperature. Then, **BL-20** photoanode was prepared by dropping the suspensions onto

the **BVO** photoanode.

Fabrication of BAg-20 photoanode

AgCl (0.3 mg) was soaked in a mixture of 20 μL Nafion (5 wt %) and 180 μL ethanol. The mixture was treated with ultrasound for 30 min at room temperature. Then, **BAg-20** photoanode was prepared by dropping the suspensions onto the **BVO** photoanode.

Fabrication of BPW_{12}-20 photoanode

$(C_{16}H_{36}N)_3PW_{12}O_{40}$ (3.1 mg) was immersed in a mixture of 20 μL Nafion (5 wt %) and 180 μL ethanol. The mixture was treated with ultrasound for 30 min at room temperature. Then, **BPW_{12}-20** photoanode was prepared by dropping the suspensions onto the **BVO** photoanode.

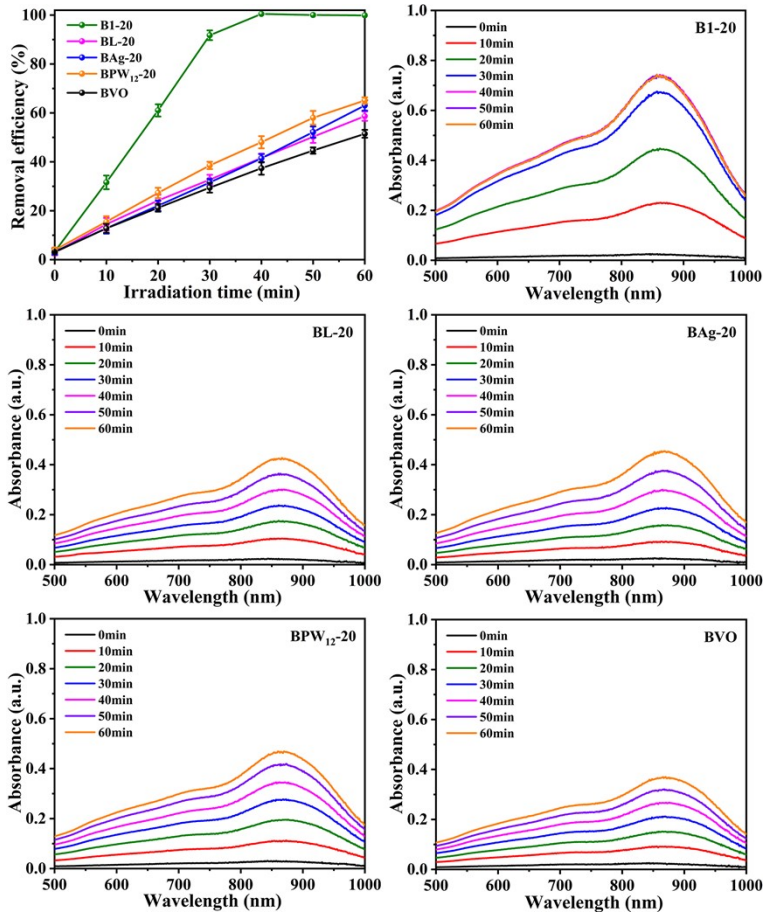

Fig. S8 Removal efficiency of As(III) and UV-visible absorption spectra of As(V) during the photoelectrocatalytic process with different photoanodes (**B1-20**, **BL-20**, **BAg-20**, **BPW$_{12}$-20** and **BVO)**.

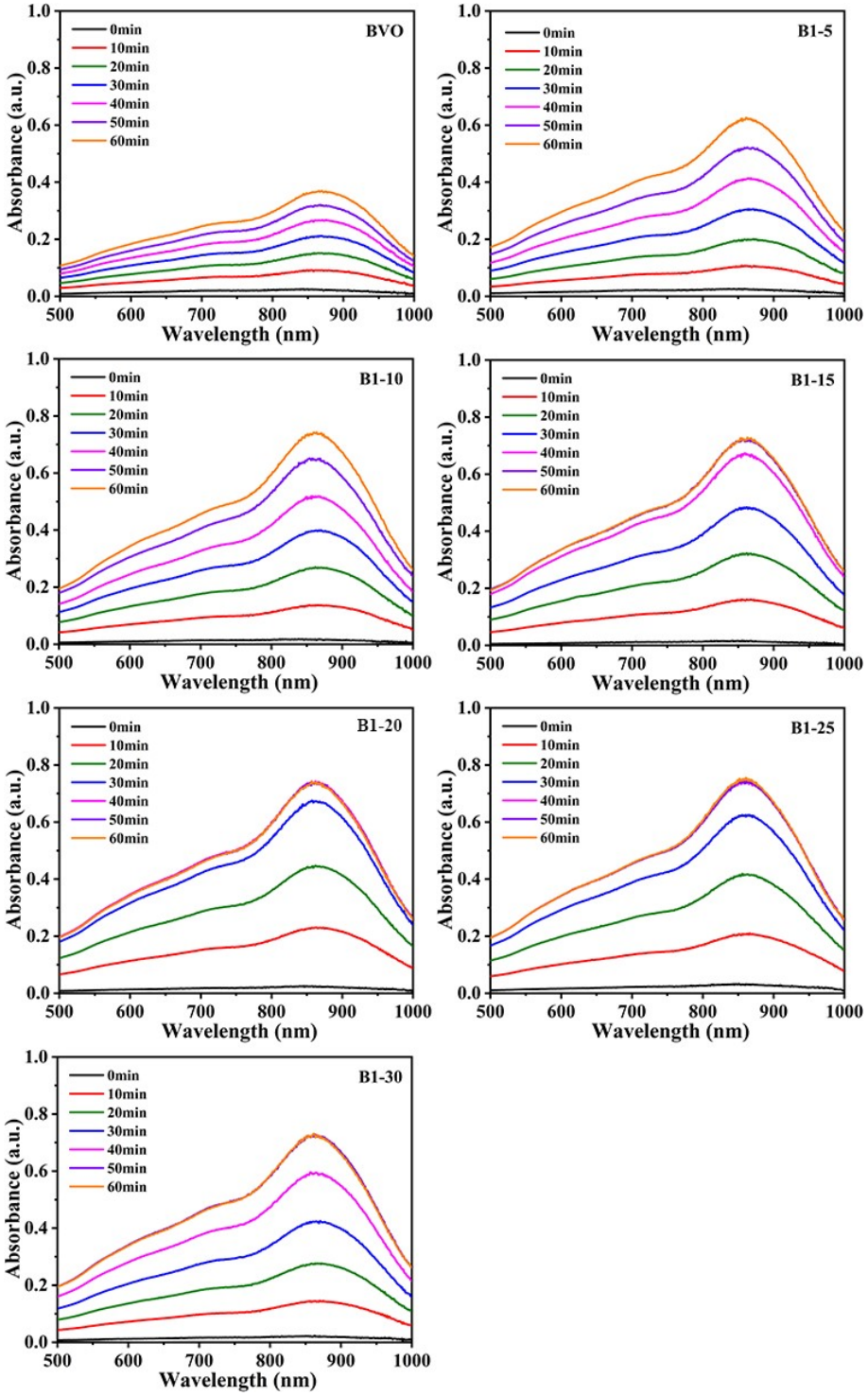

Fig. S9 UV-visible absorption spectra of As(V) during the photoelectrocatalytic process with different loading amounts of **1**.

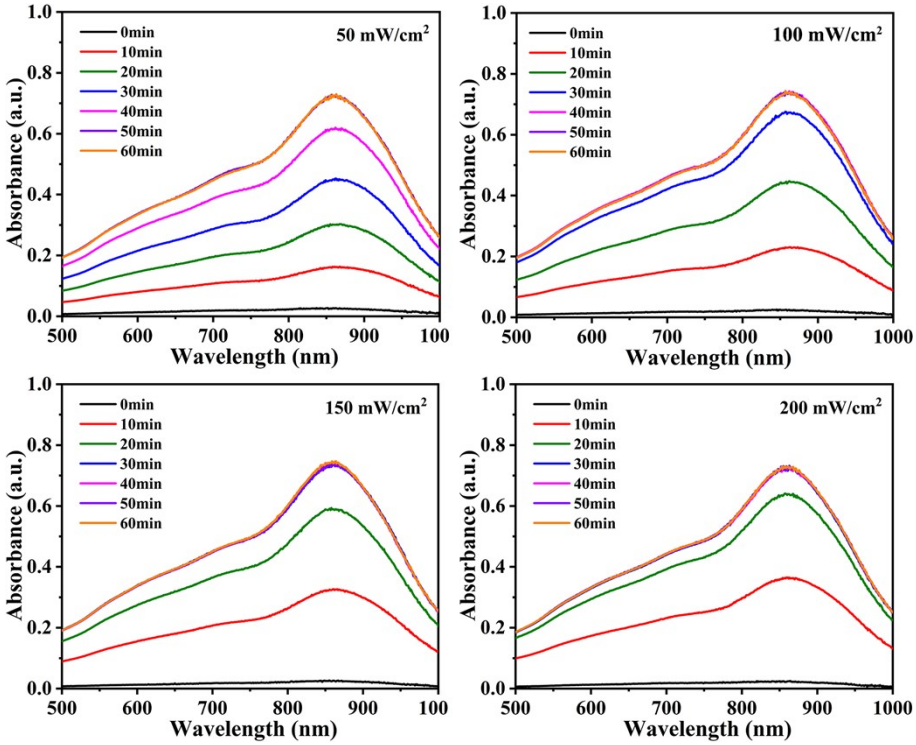

Fig. S10 UV-visible absorption spectra of As(V) during the photoelectrocatalytic process under different irradiation powers.

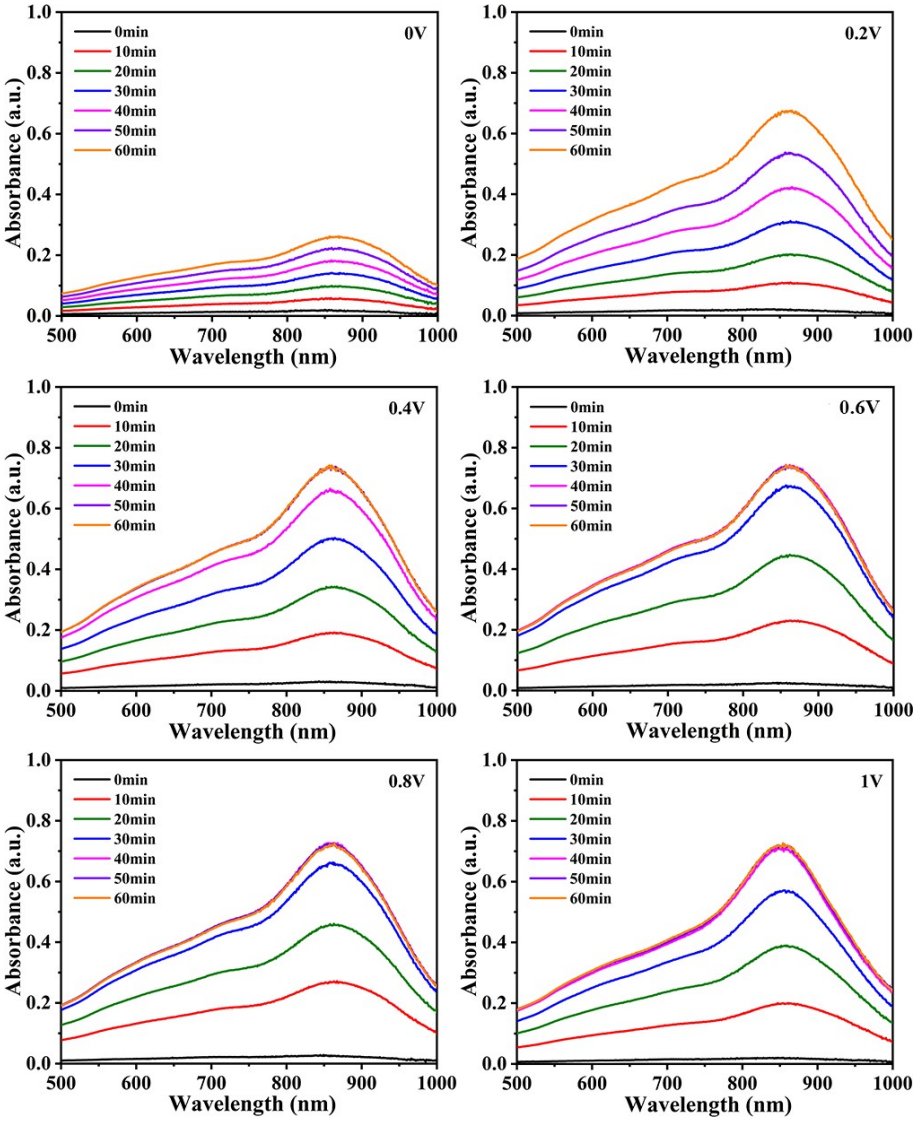

Fig. S11 UV-visible absorption spectra of As(V) during the photoelectrocatalytic process at different potentials.

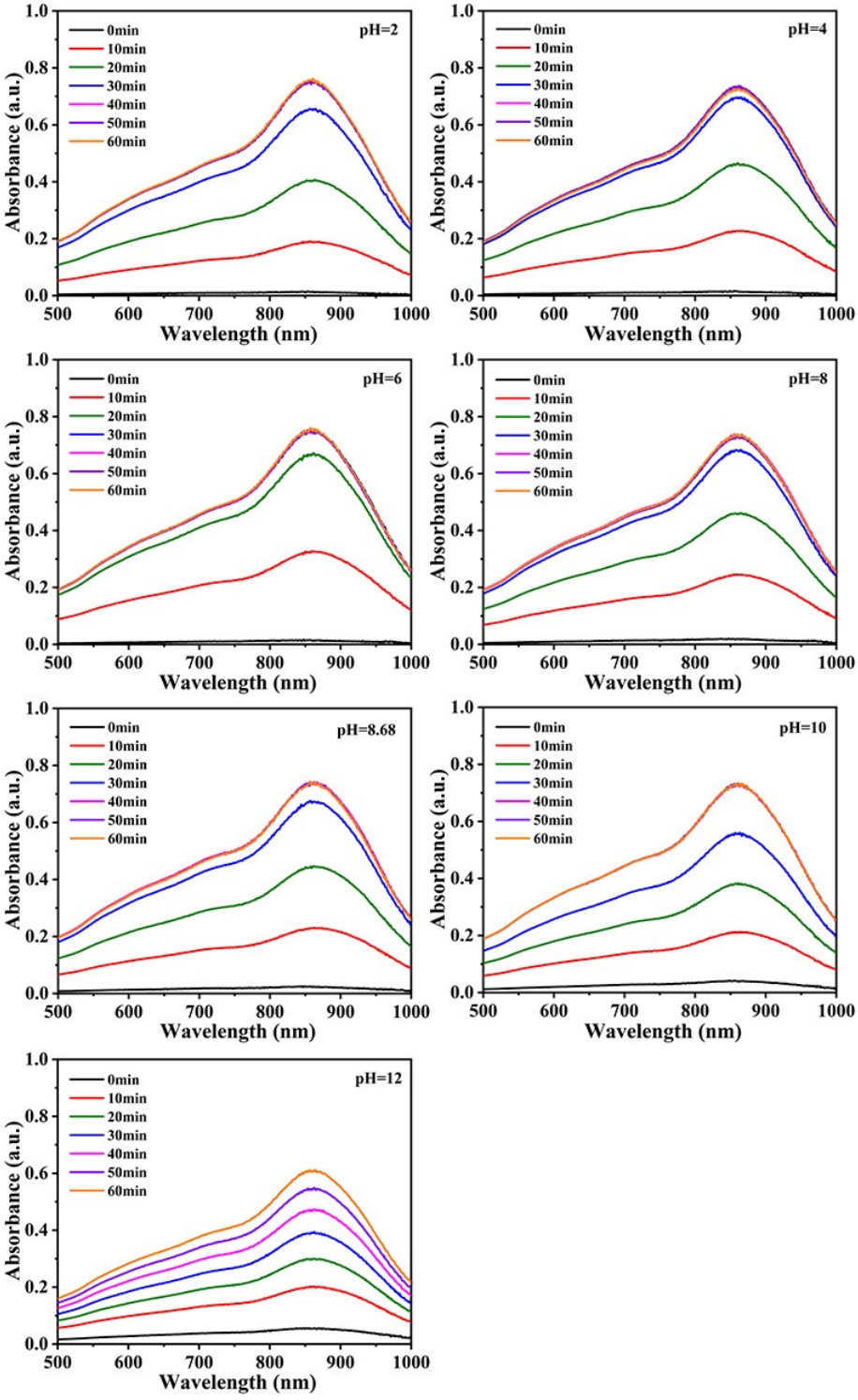

Fig. S12 UV-visible absorption spectra of As(V) during the photoelectrocatalytic process at different pH values.

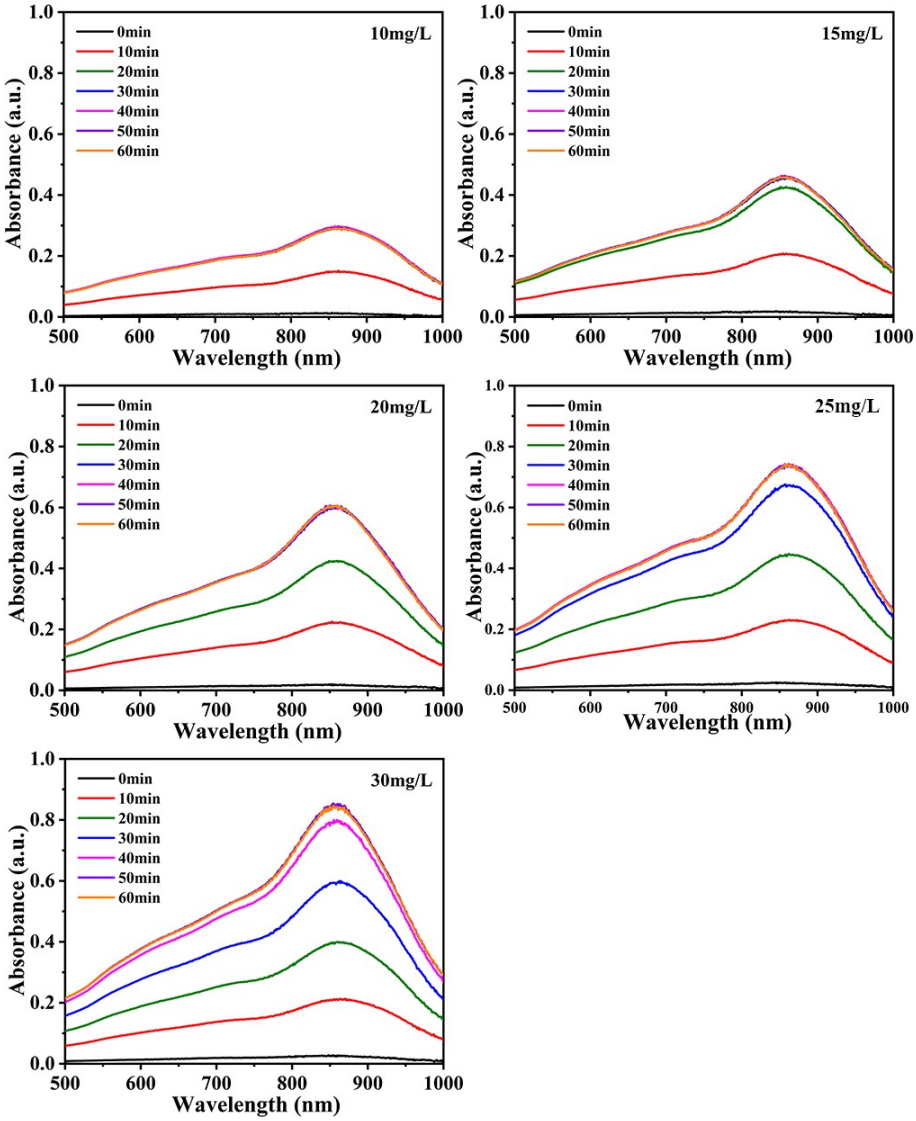

Fig. S13 UV-visible absorption spectra of As(V) during the photoelectrocatalytic process at different initial concentrations of As(III).

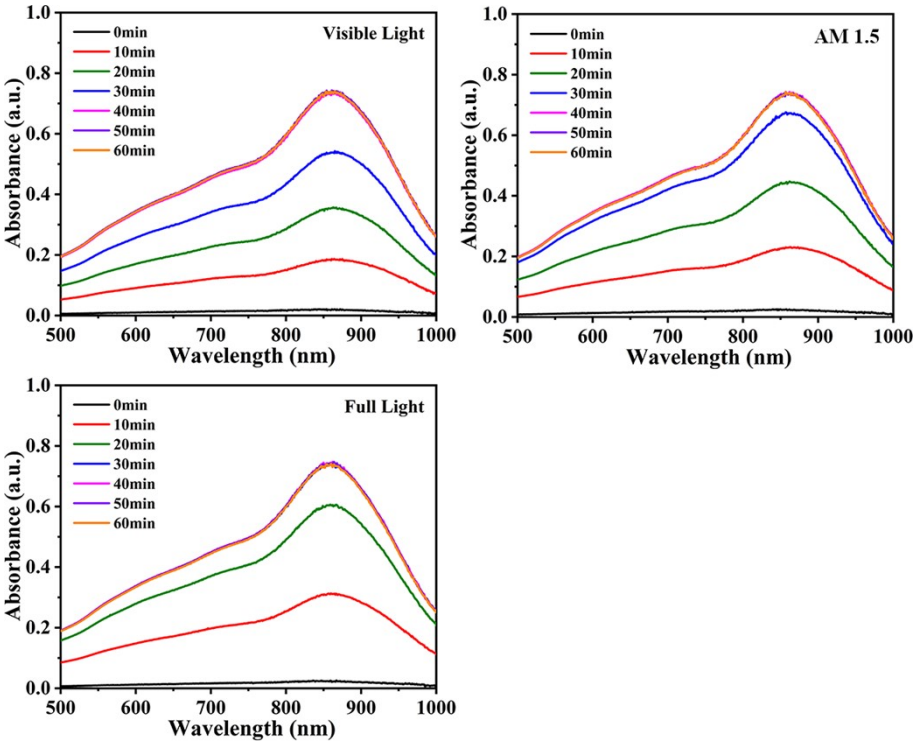

Fig. S14 UV-visible absorption spectra of As(V) during the photoelectrocatalytic process at different irradiation sources.

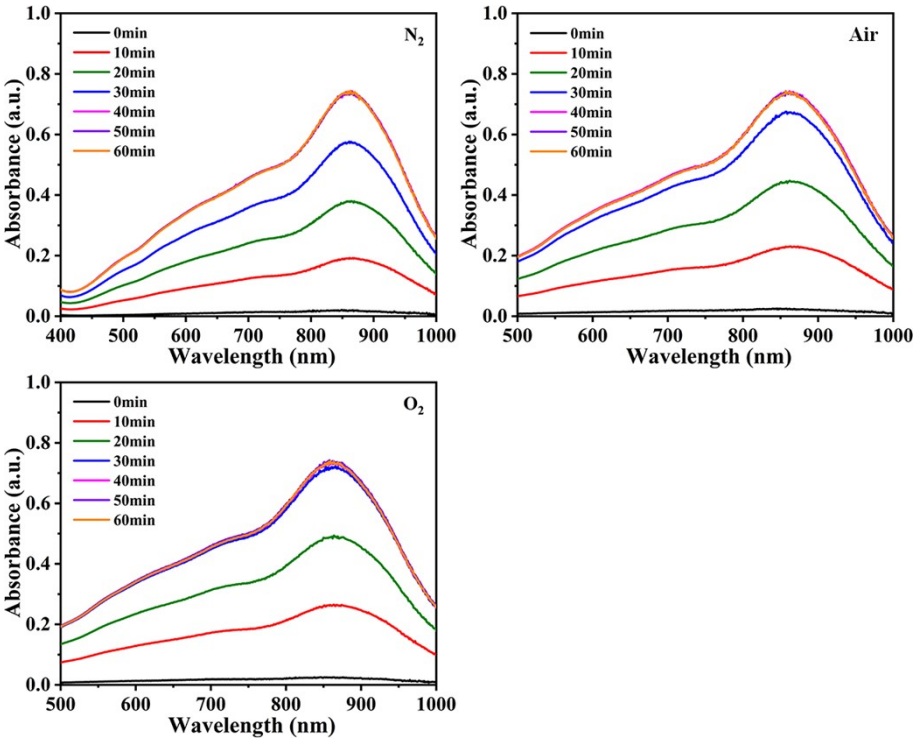

Fig. S15 UV-visible absorption spectra of As(V) during the photoelectrocatalytic process under different atmospheres.

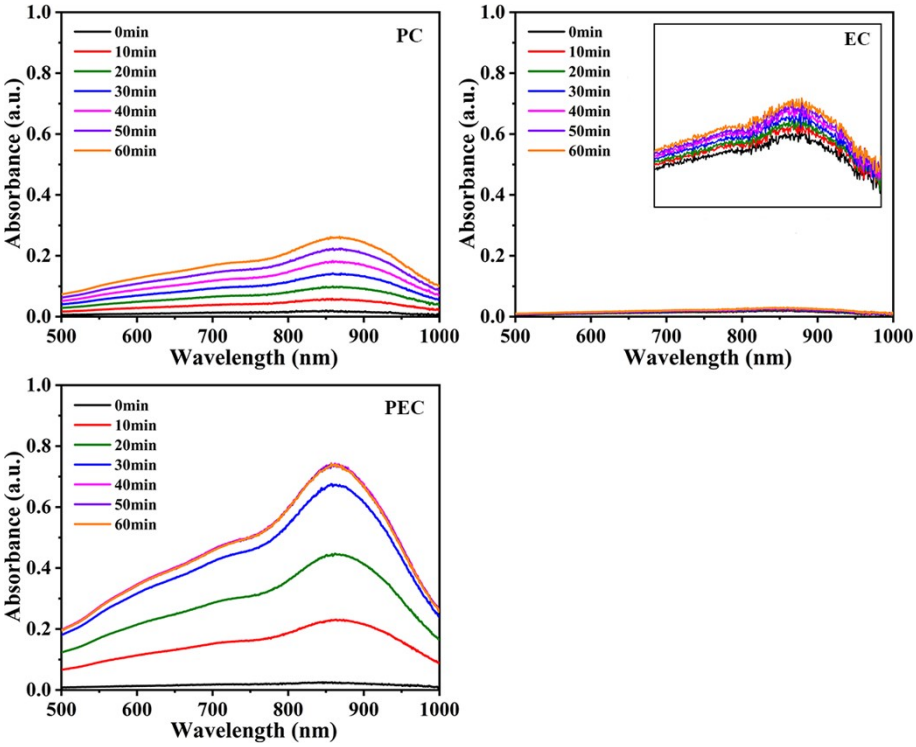

Fig. S16 UV-visible absorption spectra of As(V) during the oxidation reaction in different processes.

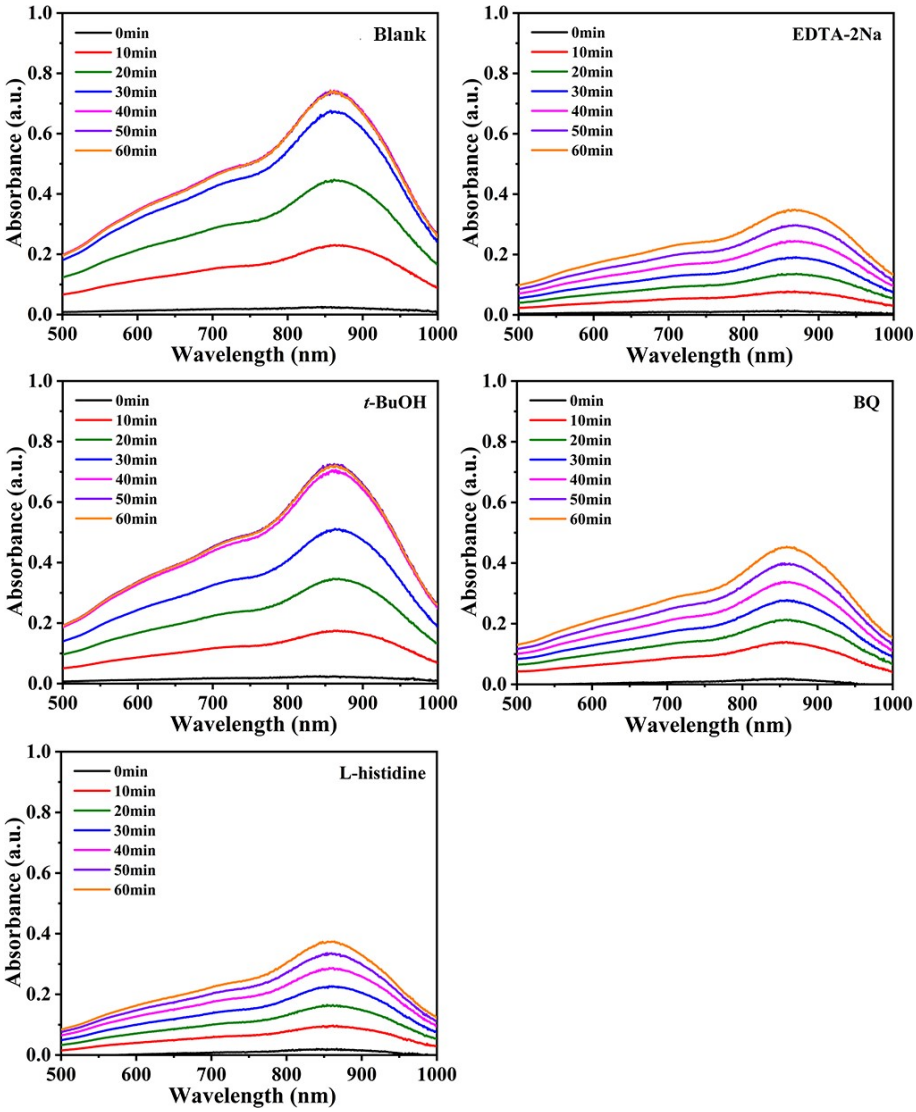

Fig. S17 UV-visible absorption spectra of As(V) during the photoelectrocatalytic process after adding different scavengers.

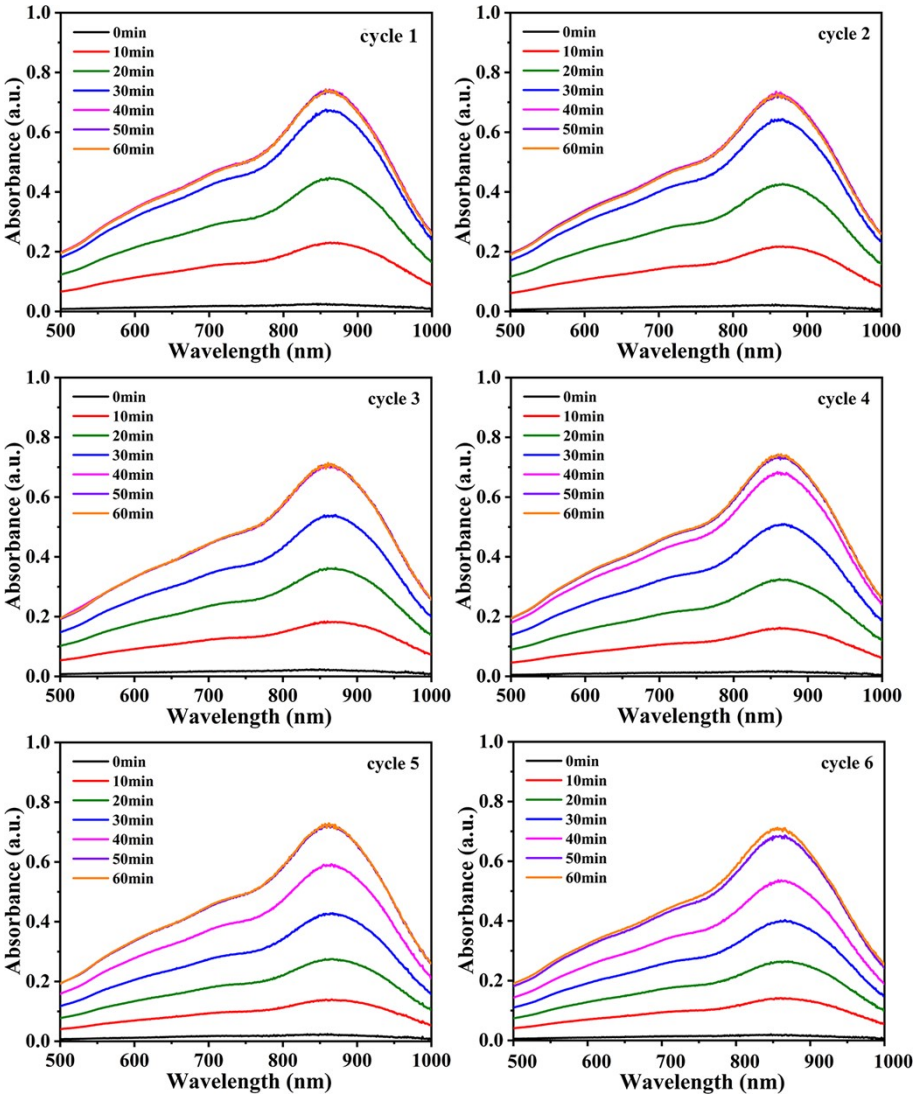

Fig. S18 UV-visible absorption spectra of the cycle experiments.

Table S1 Comparison of As(III) removal efficiency with different catalysts.

Entry	As(III) (mg/L)	Catalyst	Light source	pH	Electrolyte	removal efficiency	Time (min)	Technology	Ref.
1	25	**B1-20**	simulated sunlight	6	Na_2SO_4	100%	30	PEC	This work
2	2	V_2O_5 /TiO_2	visible light	4	-	93%	80	PC	14
3	3.4	Pt/TiO_2	visible light	7	Na_2SO_4	100%	275	PEC	15
4	2	Ag @AgCl	visible light	7	-	76%	120	PC	16

5	13	carbon-sphere@Fe_3O_4	simulated sunlight	7.3	-	20%	60	PC	17
6	25	CdS /PMo_3W_9	visible light	-	Na_2SO_4	48%	180	PEC	18
7	10	Cu_2O @TiO_2	visible light	7	NaCl	95%	30	PEC	19
8	7.8	$ZnFe_2O_4$ /g-C_3N_4	visible light	7	-	100%	120	PC	20
9	10	Bentonite /g-C_3N_4	full light	8.5	-	100%	180	PC	21
10	10	$Bi_{0.9}La_{0.1}OI$	visible light	5.7	-	60%	180	PC	22
11	50	Au-WS_2	visible light	-	Na_2SO_4	92%	120	PEC	23

Table S2 Crystallographic data for **1**.

Compound	**1**
Formula	$C_{120}H_{163}Ag_2N_{34}O_{50}PS_{16}W_{12}$
Mr	5847.70
Crystal system	*P*-1
Space group	Triclinic
a (Å)	12.6937(6)
b (Å)	18.4490(8)
c (Å)	19.5975(7)
α(°)	75.711(4)
β(°)	77.491(4)
γ(°)	88.110(4)
V(Å^3)	4340.9(3)
Z	1
D_{calc} (g·cm^{-3})	2.237

$F(000)$	2774
R_{int}	0.0541
GOF on F^2	1.055
$R_1{}^a$ [I>2σ(I)]	0.0556
$wR_2{}^b$ (all data)	0.1277

$^aR_1 = \sum||F_o| - |F_c||/\sum|F_o|$. $^bwR_2 = \{\sum w[(F_o)^2 - (F_c)^2]^2/\sum w[(F_o)^2]^2\}^{1/2}$

Table S3 Selected bond lengths [Å] and angles [°] for **1**.

Ag(1)-S(8)	2.707(4)	Ag(1)-N(6)$^{\#2}$	2.300(14)
Ag(1)-N(1)	2.262(10)	Ag(1)-N(16)$^{\#3}$	2.384(18)
N(1)-Ag(1)-S(8)	127.4(3)	N(6)$^{\#2}$-Ag(1)-S(8)	98.0(3)
N(1)-Ag(1)-N(6)$^{\#2}$	120.2(5)	N(6)$^{\#2}$-Ag(1)-N(16)$^{\#3}$	126.0(6)
N(1)-Ag(1)-N(16)$^{\#3}$	92.6(6)	N(16)$^{\#3}$-Ag(1)-S(8)	92.1(3)

Symmetry codes: $^{\#2}$ x+1,y,z, $^{\#3}$ -x+2,-y,-z+1.

Table S4 Hydrogen bonds for **1** (Å and °).

D-H...A	d(D-H)	d(H...A)	d(D...A)	<(DHA)
C(1)-H(1B)...O(13)$^{\#2}$	0.96	2.56	3.204(19)	124.5
C(1)-H(1C)...O(8)	0.96	2.6	3.299(18)	129.7
C(1)-H(1C)...O(23)	0.96	2.73	3.320(17)	120.6
C(3)-H(3A)...O(25)	0.97	2.5	3.354(14)	146.7
C(4)-H(4B)...O(4)	0.97	2.79	3.391(15)	121.1
C(15)-H(15B)...O(23)$^{\#5}$	0.96	2.55	3.360(19)	142.6
C(34)-H(34)...O(10)$^{\#6}$	0.93	2.39	3.270(17)	156.9
C(39)-H(39A)...N(8)	0.97	2.62	3.24(2)	122.4

C(55)-H(55C)...N(9)	0.96	2.46	3.32(4)	149.7

Symmetry code for **1**: #2 x+1,y,z, #5 x,y,z+1, #6 -x+1,-y+1,-z+1.

References

1 G. M. Sheldrick, SHELXS-2018, Programs for X-ray Crystal Structure Solution; University of Göttingen: Göttingen, Germany, 2018.

2 L. J. Farrugia, WINGX: A Windows Program for Crystal Structure Analysis; University of Glasgow: Glasgow, UK, 1988.

3 G. M. Sheldrick, SHELXTL-2018, Programs for X-ray Crystal Structure Refinement; University of Göttingen: Göttingen, Germany, 2018.

4 A. L. Spek, *Acta Crystallogr. Sect. C-Struct. Chem.*, 2015, **71**, 9-18.

5 J. Li, P. Du, Y. Y. Liu and J. F. Ma, *Dalton Trans.*, 2021, **50**, 1349-1356.

6 N. An, L. Zhou, W. Li, X. Yuan, L. Zhao, J. Huang, Y. Zhang, H. She, L. Wang and Q. Wang, *Appl. Catal. B Environ.*, 2022, **318**, 121869.

7 M. Navarrete-Magana, A. Estrella-Gonzalez, L. May-Ix, S. Cipagauta-Diaz and R. Gomez, *J. Environ. Manage.*, 2021, **282**, 111602.

8 M. Asadi, K. Kim, C. Liu, A. V. Addepalli, P. Abbasi, P. Yasaei, P. Phillips, A. Behranginia, J. M. Cerrato, R. Haasch, P. Zapol, B. Kumar, R. F. Klie, J. Abiade, L. A. Curtiss and A. Salehi-Khojin, *Science*, 2016, **353**, 467-470.

9 G. Kresse and J. Furthmüller, *Phys. Rev. B*, 1996, **54**, 11169-11186.

10 P. E. Blöchl, *Phys. Rev. B*, 1994, **50**, 17953-17979.

11 J. P. Perdew, K. Burke and M. Ernzerhof, *Phys. Rev. Lett.*, 1996, **77**, 3865-3868.

12 H. J. Monkhorst and J. D. Pack, *Phys. Rev. B*, 1976, **13**, 5188-5192.

13 S. Grimme, J. Antony, S. Ehrlich and H. Krieg, *J. Chem. Phys.*, 2010, **132**, 154104.

14 L. Xie, P. Liu, Z. Zheng, S. Weng and J. Huang, *Appl. Catal. B Environ.*, 2016, **184**, 347-354.

15 Y. Qin, Y. Li, Z. Tian, Y. Wu and Y. Cui, *Nanoscale Res. Lett.*, 2016, **11**, 32.

16 Y. Qin, Y. Cui, Z. Tian, Y. Wu and Y. Li, *Nanoscale Res. Lett.*, 2017, **12**, 247.

17 F. Liu, W. Zhang, L. Tao, B. Hao and J. Zhang, *Environ. Sci. Nano*, 2019, **6**, 937-947.

18 Y. Song, W. Fang, C. Liu, Z. Sun, F. Li and L. Xu, *J. Phys. Chem. Solids*, 2020, **141**, 109395.

19 W. Ji, Y. Wang, T. C. Zhang, L. Ouyang and S. Yuan, *Ind. Eng. Chem. Res.*, 2021, **60**, 17545-17555.

20 D. Lei, J. Xue, X. Peng, S. Li, Q. Bi, C. Tang and L. Zhang, *Appl. Catal. B Environ.*, 2021, **282**, 119578.

21 C. Wang, Y. Dai, X. Fu, H. Lu and J. Zhang, *Surf. Interfaces*, 2021, **26**, 101365.

22 Z. Li, L. Wu, M. Chen, Q. Zhang, S. Dai and T. Zhao, *Appl. Surf. Sci.*, 2022, **602**, 154250.

23 G. Bharath, K. Rambabu, B. Alqassem, P. P. Morajkar, M. Abu Haija, A. K. Nadda, V. K. Gupta and F. Banat, *Chem. Eng. J.*, 2023, **456**, 141062.